Superexchange theory of electronic polarization driven by relativistic spin-orbit interaction at half filling

I. V. Solovyev*

International Center for Materials Nanoarchitectonics, National Institute for Materials Science, 1-1 Namiki, Tsukuba, Ibaraki 305-0044, Japan

and Department of Theoretical Physics and Applied Mathematics, Ural Federal University, Mira str. 19, 620002 Ekaterinburg, Russia

(Received 10 March 2017; published 9 June 2017)

By applying Berry-phase theory for the effective half-filled Hubbard model, we derive an analytical expression for the electronic polarization driven by the relativistic spin-orbit (SO) coupling. The model itself is constructed in the Wannier basis, using the input from first-principles electronic structure calculations in the local-density approximation, and then treated in the spirit of the superexchange theory. The obtained polarization has the following form: $\mathbf{P}_{ij} = \boldsymbol{\epsilon}_{ji}\boldsymbol{\mathcal{P}}_{ij} \cdot [\boldsymbol{e}_i \times \boldsymbol{e}_j]$, where $\boldsymbol{\epsilon}_{ji}$ is the direction of the bond $\langle ij \rangle$, $\boldsymbol{e}_i$ and $\boldsymbol{e}_j$ are the directions of spins in this bond, and $\boldsymbol{\mathcal{P}}_{ij}$ is the pseudovector containing all the information about the crystallographic symmetry of the considered system. The expression describes the ferroelectric activity in various magnets with noncollinear but otherwise nonpolar magnetic structures, which would yield no polarization without SO interaction, including the magnetoelectric (ME) effect, caused by the ferromagnetic canting of spins in magnetic field, and spin-spiral multiferroics. The abilities of this theory are demonstrated for the analysis of linear ME effect in Cr_2O_3 and $BiFeO_3$, and the properties of multiferroics $MnWO_4$, β-MnO_2, $CuFeO_2$, and MnI_2. In all considered examples, the theory perfectly describes the symmetry properties of the induced polarization. However, in some cases, the values of this polarization are underestimated, suggesting that other effects, besides the spin and electronic ones, can also play an important role.

DOI: 10.1103/PhysRevB.95.214406

I. INTRODUCTION

The relativistic spin-orbit (SO) interactions is responsible for many spectacular phenomena in condensed matter physics, which are widely employed in many technological applications. Particularly, being a natural mechanism connecting spin and orbital degrees of freedom, it provides a unique possibility for the mutual control of various spin and lattice-related properties. Every year, growing interest in this problem leads to the discovery of new and more sophisticated schemes of such control [1].

One of the interesting topics is the effect of the SO coupling in noncentrosymmetric substances. In magnetic systems, it leads to the famous antisymmetric Dzyaloshinskii-Moriya (DM) interaction $\boldsymbol{d}_{ij} \cdot [\boldsymbol{e}_i \times \boldsymbol{e}_j]$ between spins in the noncentrosymmetric bond $\langle ij \rangle$, where $\boldsymbol{e}_i$ and $\boldsymbol{e}_j$ are the directions of these spins [2,3]. On many occasions, the DM interactions result in spin canting and noncollinear magnetic order. However, one can also look at this situation from the opposite side: suppose there is a noncollinear arrangement of spins, which is produced by other means, such as an external magnetic field or frustrated magnetic interactions of nonrelativistic origin. Then, in some magnetic architectures, this noncollinear arrangement can break the inversion symmetry, which will immediately manifest itself in the ferroelectric (FE) activity. The canonical example of such activity is the magnetoelectric (ME) effect, where the noncollinearity is induced by the external magnetic field [4]. The interest in this problem has reemerged a decade ago, after the discovery of a new generation of multiferroic materials, where the FE activity is triggered by some massive change of the magnetic structure, which breaks spontaneously the inversion symmetry [5]. Nevertheless, the microscopic understanding of mechanisms resulting in finite electric polarization is still far from being complete, even despite significant progress in this direction.

Historically, the first phenomenological expression for the electric polarization induced by the noncollinear spin order was introduced by Moriya in 1968 on the basis of general symmetry considerations [6]: in each magnetic bond, such polarization

$$P^a_{ij} = \sum_b \mathsf{d}^{ab}_{ij} [\boldsymbol{e}_i \times \boldsymbol{e}_j]^b, \tag{1}$$

has the same form as the DM exchange interaction, where the vector $\boldsymbol{d}_{ij}$ is replaced by the tensor d^{ab}_{ij} with a and b denoting x, y, or z.

The first microscopic derivation of the electric polarization driven by the relativistic SO coupling in noncollinear magnetic substances was undertaken by Katsura, Nagaosa, and Balatsky (KNB) [7]. However, it should be understood that the KNB model deals with a very special example of electronic structure, consisting of the transition-metal (TM) t_{2g} levels with some particular scheme of filling, which are split by the SO coupling and interact via intermediate oxygen (O) $2p$ states in the single undistorted TM-O-TM bond. Thus the analysis is hardly to be complete. Nevertheless, on the basis of these considerations, the authors of Ref. [7] have concluded that the electric polarization should behave as

$$\mathbf{P}_{ij} \propto \boldsymbol{\epsilon}_{ji} \times [\boldsymbol{e}_i \times \boldsymbol{e}_j], \tag{2}$$

where $\boldsymbol{\epsilon}_{ji}$ is the unit vector in the direction of TM site j relative to the TM site i. It is also referred to as the spin-current mechanism of the electric polarization, which is widely used today for the analysis of experimental data [5].

*SOLOVYEV.Igor@nims.go.jp

A similar conclusion was drawn in Ref. [8] on the basis of phenomenological Ginzburg-Landau theory for a cubic symmetry. Thus, expression (2) does not depend on the specific crystallographic symmetry of considered compounds, so that one can have a wrong impression that the electric polarization in all noncollinear magnets should behave in a similar way. It clearly contrasts with the DM interaction $\boldsymbol{d}_{ij}$, which does depend on the symmetry. Nevertheless, this expression is formally consistent with the general definition (1) given by Moriya and can be reduced to it if $\mathsf{d}_{ij}^{ab} = -\varepsilon_{abc}\epsilon_{ji}^{c}$, where ε_{abc} is the antisymmetric symbol of Levi-Civita. The spin-current mechanism frequently tends to be identified with the inverse DM mechanism, proposed in Ref. [9]: similar to how the off-centrosymmetric oxygen displacement in the bond TM-O-TM gives rise to the noncollinear alignment of spins [2,3], one can expect the opposite (magnetostrictive-like) effect, where the noncollinear magnetic alignment should lead to the off-centrosymmetric atomic displacement. However, it should be understood that these mechanisms are quite different (though complementary to each other): Ref. [7] deals with the purely electronic effect, while Ref. [9] deals with the lattice effect.

There are several examples where the KNB theory fails to explain the experimental behavior of the electric polarization. It has never been applied to the analysis of the ME effect, though the ferromagnetic (FM) canting of spins, which is responsible for this effect, is one of the possible types of the noncollinear magnetic arrangement and, therefore, the induced electric polarization should be describable by some proper spin-current theory. Furthermore, there are several multiferroic materials (e.g., $CuFeO_2$ [10] and MnI_2 [11]), which exhibit proper-screw type magnetic order ($\boldsymbol{\epsilon}_{ji}||[\boldsymbol{e}_i \times \boldsymbol{e}_j]$), where the KNB theory predicts no net polarization, contrary to the experimental evidence. This urged several authors to generalize the KNB theory, also on a phenomenological basis. Arima [10] has considered single-ion contributions (also predicted by Moriya [6]) caused by the SO-dependent change of the TM-O hybridization. However, if the magnetic TM ion is located in the inversion center (like in $CuFeO_2$ and MnI_2), such contributions are expected to vanish [6], as it also follows from the modern formulation [12] based on the Berry-phase theory [13–15]. Xiang *et al.* [16] have basically considered the general expression proposed by Moriya [6] (both single-ion and bond contribution) and fit all the coefficients using the input from first-principles calculations with constrained directions of the magnetic moments.

The most rigorous theoretical basis for the analysis of electronic polarization is provided by the Berry-phase theory, which relates the polarization with the expectation value of the position operator in the basis of localized Wannier functions for the occupied states [13–15]:

$$\mathbf{P} = -\frac{e}{V}\int \mathbf{r}\, w^2(\mathbf{r})\, d\mathbf{r}, \tag{3}$$

where $-e < 0$ is the electron charge, V is the unit-cell volume, and $w^2(\mathbf{r}) = \sum_{n=1}^{M} |W_n(\mathbf{r})|^2$ is the total weight of the Wannier functions for the M occupied states. Each Wannier function is centered near a certain site of the lattice and can have tails spreading to the neighboring sites. The relative weight of these tails depends on the magnetic state. This is how the Wannier function bears the information about the magnetic configuration at the neighboring sites. Thus the understanding of magnetic-state dependence of the electronic polarization is essentially the understanding of how the magnetic order and relativistic SO interaction leads to the asymmetric deformation of the Wannier functions around each magnetic site [17–19]. It should not be confused with the asymmetric distribution of the electron density, which includes the contributions of several Wannier functions centered at different sites and, therefore, leads to the incorrect answer [13,14].

In our previous work [18], we have applied this strategy to the analysis of electronic polarization caused by the nonrelativistic double exchange mechanism in multiferroic manganites. In that case, competing magnetic interactions of both relativistic and nonrelativistic origin result in highly asymmetric magnetic structure, which breaks the inversion symmetry. The SO interaction plays an important role in this asymmetry by deforming the homogeneous spin-spiral texture [18,20] (the so-called bunching effect due to the single-ion anisotropy [21]). This deformation gives rise to the polarization $\mathbf{P}_{ij} \propto (\boldsymbol{e}_i \cdot \boldsymbol{e}_j)$, which depends on the SO coupling only indirectly, via the noncentrosymmetric distribution of spins, while the proportionality coefficient between $\mathbf{P}_{ij}$ and $(\boldsymbol{e}_i \cdot \boldsymbol{e}_j)$ does not depend on the SO coupling. This double exchange mechanism has allowed us to rationalize many aspects of the electric polarization in multiferroic manganites [18].

In this paper, we consider the proper spin-current mechanism. In some sense, the situation is the opposite to the double exchange mechanism, considered in Ref. [18]. Namely, we will deal with some noncollinear magnetic structures, which are stabilized by nonrelativistic means: it can be either the spin-spiral structure arising from the competition of several isotropic exchange interactions or a canted spin structure, inherent to the ME effect, where the collinear antiferromagnetic (AFM) order is deformed by the magnetic field. Without SO coupling all these magnetic structures can be transformed to themselves by combining the spacial inversion with some appropriate rotation of the spin system as the whole [22]. Therefore the electric polarization will vanish. Nevertheless, the situation may change after switching on the SO coupling, which does not deform the spin texture itself (or, at least, such deformation can be neglected), but can deform the Wannier functions, resulting in their asymmetry and finite electronic polarization.

In our analysis, we use the effective Hubbard model derived from the first-principles electronic structure calculations and the local-density approximation (LDA) as the starting point for such derivation [23]. We consider the simplest case of the half filling, which also allows us to get rid of additional complications related to the orbital degrees of freedom. Furthermore, the on-site Coulomb repulsion is the largest parameter in our model, so that other parameters can be treated as a perturbation in the spirit of the superexchange (SE) theory [24]. We will use this strategy in order to derive an analytical expression for the DM exchange interactions and electronic polarization. We will show that in the first order of the SO coupling the correct expression for the electronic polarization in the framework of the Berry-phase theory [13,14] has the following form:

$$\mathbf{P}_{ij} = \boldsymbol{\epsilon}_{ji}\boldsymbol{\mathcal{P}}_{ij} \cdot [\boldsymbol{e}_i \times \boldsymbol{e}_j], \tag{4}$$

where the pseudovector $\mathcal{P}_{ij}$ contains all the information about the individual symmetry of the lattice. Thus there is at least one important addition to the phenomenological expression (2): the polarization does depend on the symmetry of the lattice, as it should be. In terms of Moriya's definition [6], the tensor d_{ij}^{ab} is now given by $\mathsf{d}_{ij}^{ab} = \epsilon_{ji}^{a}\mathcal{P}_{ij}^{b}$. We will show that this expression is very general and describes not only the behavior of polarization in various spin-spiral magnets, but also the ME effect caused by the FM canting of spins in otherwise collinear AFM state of a special symmetry.

Another important issue is whether the spin-current mechanism alone is able to reproduce experimental values of the ME effect and electric polarization in real materials. Additional mechanisms, which are widely discussed in the literature, are the lattice deformation [25–27] (in line with the proposal [9]), orbital contribution to the ME coupling [26,28], and hidden deformation of the magnetic texture with broken inversion symmetry [20,22]. By using realistic model, derived from the first-principles calculations, we will show that the situation can be very different. In some cases, the spin-current mechanism alone reproduces the experimental polarization reasonably well. In other cases (e.g., in Cr_2O_3), it captures only the symmetry properties of the polarization, while the numerical values can be off by several order of magnitude, suggesting the importance of other mechanisms [26–28]. But, generally, the lattice distortion is expected to play some role in all considered examples [22]

The rest of the paper is organized as follows. In Sec. II, we will present our formalism based on the SE theory, which is applied to antisymmetric DM exchange interactions and electric polarization in Secs. II A and II B, respectively. The details of these derivations are given in Ref. [29]. In Sec. III, we will consider practical applications of this formalism to the linear ME effect in Cr_2O_3 and $BiFeO_3$ (Secs. III A and III B, respectively), the FE activity caused by the spin-spiral order in multiferroic $MnWO_4$ and β-MnO_2 (Secs. III C and III D, respectively), and symmetry aspects of the electric polarization in $CuFeO_2$ and MnI_2 (Sec. III E). Finally, in Sec. IV, we will summarize our work.

II. FORMALISM

In this section, we will sketch the main details of derivation of analytical expressions for the DM exchange interactions and electric polarization, following the SE theory in the lowest order of perturbation with respect to the transfer integrals $\hat{t}_{ij}$ [24]. The technical details can be found in Ref. [29]. The simplest microscopic model, capturing the physics of the spin-current mechanism, reads $\hat{H} = \hat{h} + \hat{t}$, where $\hat{h} \equiv \hat{h}_{\rm ex} + \hat{h}_{\rm cf} + \hat{h}_{\rm so}$ is the on-site part, including the interaction $\hat{h}_{\rm ex} = \frac{U}{2}\boldsymbol{e}\cdot\hat{\boldsymbol{\sigma}}$ with the internal exchange field in the direction $\boldsymbol{e} = (\sin\theta\cos\phi, \sin\theta\sin\phi, \cos\theta)$ ($\hat{\boldsymbol{\sigma}}$ being the vector of Pauli matrices), the crystal-field splitting $\hat{h}_{\rm cf}$, and the SO interaction $\hat{h}_{\rm so} = \frac{\xi}{2}\hat{\mathbf{L}}\cdot\hat{\boldsymbol{\sigma}}$, while $\hat{t} \equiv [\hat{t}_{ij}]$ is the intersite part. More specifically, $\hat{H}$ can be viewed as a mean-field Hamiltonian (for instance, the one obtained from the solution of the Hubbard model in the Hartree-Fock approximation), where $\hat{h}_{\rm ex}$ describes the averaged exchange splitting for the half-filled ionic shell, driven by the effective interaction U, and the crystal field $\hat{h}_{\rm cf}$ also includes the effects of nonsphericity of the mean-field potential. Thus, what we consider here is the canonical "spin-current" model, where the local magnetic moments are the spin ones, while the orbital magnetization contributes to neither DM interactions nor the electric polarization. The parameters of such a microscopic model, formulated in the Wannier basis [15], can be derived from the first-principles electronic structure calculations [23]. For practical purposes we use the linear muffin-tin orbital (LMTO) method [30].

The basic idea of the SE theory is to start from the atomic limit and treat $\hat{h}_{\rm so}$ and $\hat{t}$ as a perturbation. Then, the wave functions of $\hat{H}_0 = \hat{h}_{\rm ex} + \hat{h}_{\rm cf}$ for the occupied (−) and unoccupied (+) spin states are given by

$$|\Psi^-\rangle = \begin{pmatrix} -\sin\frac{\theta}{2}e^{-i\phi} \\ \cos\frac{\theta}{2}\end{pmatrix}|\Psi\rangle$$

and

$$|\Psi^+\rangle = \begin{pmatrix} \cos\frac{\theta}{2} \\ \sin\frac{\theta}{2}e^{i\phi}\end{pmatrix}|\Psi\rangle,$$

respectively, where $|\Psi\rangle$ is the column of eigenvectors of $\hat{h}_{\rm cf}$ with the eigenvalues $\{\varepsilon_n\}$. More specifically, $|\Psi\rangle$ is the M-dimensional vector in the subspace of orbital states, while $|\Psi^\pm\rangle$ are $2M$-dimensional vectors in the space of spin and orbital states. Then, the corresponding eigenvectors in the first order of the SO interaction will be given by

$$|\tilde{\Psi}^-\rangle = |\Psi^-\rangle - \bar{\xi}|\Psi^+\rangle\langle\Psi^+|(\hat{\mathbf{L}} - [\hat{\tilde{h}}_{\rm cf},\hat{\mathbf{L}}])\cdot\hat{\mathbf{S}}|\Psi^-\rangle$$

and

$$|\tilde{\Psi}^+\rangle = |\Psi^+\rangle + \bar{\xi}|\Psi^-\rangle\langle\Psi^-|(\hat{\mathbf{L}} + [\hat{\tilde{h}}_{\rm cf},\hat{\mathbf{L}}])\cdot\hat{\mathbf{S}}|\Psi^+\rangle,$$

where $\bar{\xi} = \xi/U$, $\hat{\tilde{h}}_{\rm cf} = \hat{h}_{\rm cf}/U$, and $[\hat{A},\hat{B}] = \hat{A}\hat{B} - \hat{B}\hat{A}$. Moreover, in the conventional perturbation theory expression, we further expand $(\varepsilon_n - \varepsilon_m \pm U)^{-1}$ with respect to $\hat{\tilde{h}}_{\rm cf}$. Then, the first term in $(\hat{\mathbf{L}} \mp [\hat{\tilde{h}}_{\rm cf},\hat{\mathbf{L}}])$ corresponds to $\hat{h}_{\rm cf} = 0$ (apart from the constant energy shift), while the second terms appear in the first order of $\hat{\tilde{h}}_{\rm cf}$. In practical calculations, we use the effective ξ, which also incorporates the change of the Coulomb and exchange potential in the first order of the SO interaction, as obtained in the self-consistent linear response (SCLR) theory [31].

A. Exchange interactions

The exchange interactions in the bond $\langle ij\rangle$ describe the energy change δE_{ij} in the second order of $\hat{\tilde{t}}_{ij} = \hat{t}_{ij}/U$, where the transfer integrals connect the occupied and unoccupied states of the sites i and j:

$$\delta E_{ij} \simeq -U\langle\tilde{\Psi}_i^-|\hat{\tilde{t}}_{ij} + \tfrac{1}{2}[\hat{\tilde{h}}_{\rm cf},\hat{\tilde{t}}_{ij}]|\tilde{\Psi}_j^+\rangle\langle\tilde{\Psi}_j^+|\hat{\tilde{t}}_{ji} - \tfrac{1}{2}[\hat{\tilde{h}}_{\rm cf},\hat{\tilde{t}}_{ji}]|\tilde{\Psi}_i^-\rangle + (i \leftrightarrow j).$$

This expression is also valid in the first order of $\hat{\tilde{h}}_{\rm cf}$. Then, after tedious but rather straightforward algebra, it can be rearranged as (see Ref. [29] for details)

$$\delta E_{ij} \simeq J_{ij}(1 - \boldsymbol{e}_i\cdot\boldsymbol{e}_j) + \boldsymbol{d}_{ij}\cdot[\boldsymbol{e}_i\times\boldsymbol{e}_j], \qquad (5)$$

where

$$J_{ij} = -U\mathrm{Tr}_L\{\hat{\bar{t}}_{ij}\hat{\bar{t}}_{ji}\} \quad (6)$$

is the isotropic exchange coupling, which does not depend on the SO interaction, and

$$\boldsymbol{d}_{ij} = \xi\mathrm{Tr}_L\{\hat{\bar{t}}_{ij}[[\hat{\bar{h}}_{\mathrm{cf}},i\hat{\mathbf{L}}],\hat{\bar{t}}_{ji}]\} \quad (7)$$

is the DM coupling, which appears in the first order of ξ. Other exchange interactions, including the symmetric anisotropic one, appear in higher orders of ξ. Tr_L in Eqs. (6) and (7) denotes the trace over M orbital indices.

Finally, we note the following properties. (i) $\boldsymbol{d}_{ij}$ is the antisymmetric pseudovector: $\hat{I}\boldsymbol{d}_{ij} = \boldsymbol{d}_{ij}$, and $\boldsymbol{d}_{ji} = -\boldsymbol{d}_{ij}$. (ii) The values of the DM interactions depend on the crystal-field splitting and vanish when $\hat{\bar{h}}_{\mathrm{cf}} = 0$ (again, apart from the constant energy shift). Then, Eq. (7) can be interpreted in the following way: since $[\hat{\bar{h}}_{\mathrm{cf}},i\hat{\mathbf{L}}]$ is the measure of unquenched orbital magnetization (or the observable orbital magnetization in the presence of the crystal field), the DM interaction $\boldsymbol{d}_{ij}$ is a probe of the orbital magnetization at the site j by the electron hoppings from the site i (and vice versa).

B. Electronic polarization

We start with the general expression for the electric polarization (3) in terms of the Wannier functions for the occupied states. Then, we adopt it for the lattice model by assuming that all weights of w are localized in the lattice points: i.e., if w_i are the occupied Wannier functions centered at the site i, their weights are distributed as

$$w_i^2(\mathbf{r}) = \sum_j w_{ij}^2\,\delta(\mathbf{r} - \Delta\boldsymbol{\tau}_{ji}),$$

where $\Delta\boldsymbol{\tau}_{ji} = \boldsymbol{R}_j - \boldsymbol{R}_i$ is the position of the site j relative to the site i. Then, the electronic polarization (3) can be related to the asymmetric transfer of the weights of the Wannier functions in each bond [18]:

$$\mathbf{P} = \frac{1}{2}\sum_{ij}\mathbf{P}_{ij}, \quad (8)$$

where

$$\mathbf{P}_{ij} = -\frac{e\Delta\boldsymbol{\tau}_{ji}}{V}(w_{ij} - w_{ji}). \quad (9)$$

In the SE theory, the quantities w_{ij} are evaluated in the first order of perturbation theory for the Wannier functions with respect to $\hat{\bar{t}}_{ij}$ between occupied and unoccupied states, starting from the atomic limit:

$$w_{ij} \simeq |\langle\tilde{\Psi}_j^+|\hat{\bar{t}}_{ji} - [\hat{\bar{h}}_{\mathrm{cf}},\hat{\bar{t}}_{ji}]|\tilde{\Psi}_i^-\rangle|^2.$$

Then, using tedious but rather straightforward algebra, one can obtain the following expression for $\mathbf{P}_{ij}$ (see Ref. [29] for details):

$$\mathbf{P}_{ij} = \frac{e\Delta\boldsymbol{\tau}_{ji}}{V}\bar{\xi}\mathrm{Tr}_L\{[\hat{\bar{h}}_{\mathrm{cf}},\hat{\bar{t}}_{ij}][[\hat{\bar{h}}_{\mathrm{cf}},i\hat{\mathbf{L}}],\hat{\bar{t}}_{ji}] + [\hat{\bar{h}}_{\mathrm{cf}},\hat{\bar{t}}_{ji}][[\hat{\bar{h}}_{\mathrm{cf}},i\hat{\mathbf{L}}],\hat{\bar{t}}_{ij}]\}\cdot[\boldsymbol{e}_i\times\boldsymbol{e}_j], \quad (10)$$

which can be further rearranged as Eq. (4) with $\boldsymbol{\epsilon}_{ji} = \frac{\Delta\boldsymbol{\tau}_{ji}}{|\Delta\boldsymbol{\tau}_{ji}|}$ and

$$\boldsymbol{\mathcal{P}}_{ij} = \frac{e|\Delta\boldsymbol{\tau}_{ji}|}{V}\bar{\xi}\mathrm{Tr}_L\{[\hat{\bar{h}}_{\mathrm{cf}},\hat{\bar{t}}_{ij}][[\hat{\bar{h}}_{\mathrm{cf}},i\hat{\mathbf{L}}],\hat{\bar{t}}_{ji}] + [\hat{\bar{h}}_{\mathrm{cf}},\hat{\bar{t}}_{ji}][[\hat{\bar{h}}_{\mathrm{cf}},i\hat{\mathbf{L}}],\hat{\bar{t}}_{ij}]\}.$$

Thus we note the following. (i) Unlike $\boldsymbol{d}_{ij}$, $\boldsymbol{\mathcal{P}}_{ij}$ is the *symmetric* pseudovector: $\hat{I}\boldsymbol{\mathcal{P}}_{ij} = \boldsymbol{\mathcal{P}}_{ij}$, *while* $\boldsymbol{\mathcal{P}}_{ji} = \boldsymbol{\mathcal{P}}_{ij}$ due to the definition (9). (ii) Similar to the DM interactions, the electronic polarization crucially depends on $\hat{\bar{h}}_{\mathrm{cf}}$ and vanishes when $\hat{\bar{h}}_{\mathrm{cf}} = 0$. (iii) There is a fundamental difference from phenomenological expression (2) [7,8]. Namely, the spin-dependent cross product $[\boldsymbol{e}_i\times\boldsymbol{e}_j]$ does not couple directly to $\boldsymbol{\epsilon}_{ji}$. It couples to the pseudovector $\boldsymbol{\mathcal{P}}_{ji}$, which contains all the information about the particular crystallographic symmetry of the system. The directional dependence of $\mathbf{P}$ is specified by the vectors $\boldsymbol{\epsilon}_{ji}$, which are modulated by the scalar products $\boldsymbol{\mathcal{P}}_{ij}\cdot[\boldsymbol{e}_i\times\boldsymbol{e}_j]$. This important addition will allow us to resolve several controversies related to the symmetry properties of electric polarization induced by the noncollinear magnetic alignment.

III. RESULTS AND DISCUSSIONS

A. Perpendicular magnetoelectric effect in Cr_2O_3

We start our discussion with the canonical example of ME effect in AFM Cr_2O_3 [4], which crystallizes in corundum structure with the space group $R\bar{3}c$ [32]. The formal configuration of the Cr^{3+} ions in octahedral environment is t_{2g}^3. According to LDA calculations, the Cr t_{2g} bands are indeed well isolated and located near the Fermi level (Fig. 1). Thus, as a first approximation, we consider the simplest t_{2g} model at the half filling and apply it for the analysis of the ME effect in Cr_2O_3. The model itself is constructed in the Wannier basis as described in Ref. [23]. The obtained transfer integrals and parameters of the crystal field are set to reproduce the LDA band structure for the Cr t_{2g} bands. The matrix of screened Coulomb interactions was evaluated in the framework of

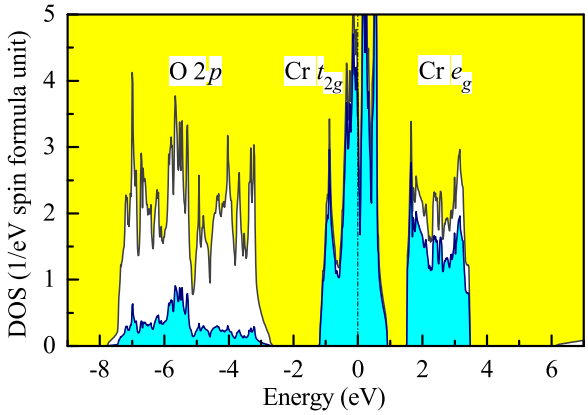

FIG. 1. Total and partial densities of states of Cr_2O_3 in the local density approximation. The shaded light (blue) area shows contributions of the Cr3d states. Positions of the main bands are indicated by symbols. The Fermi level is at zero energy (shown by dot-dashed line).

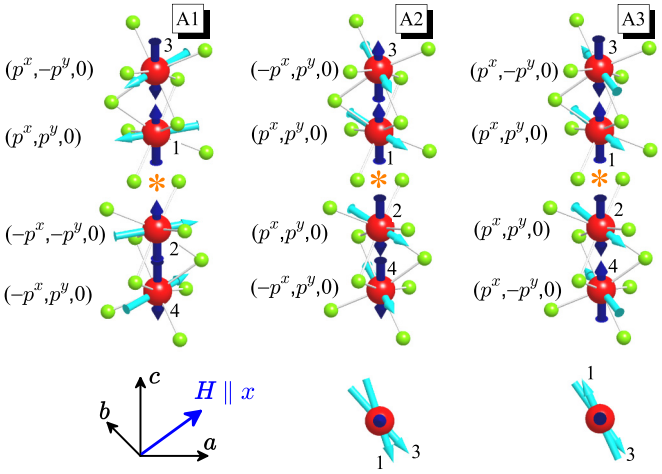

FIG. 2. Directions of electronic polarization at four Cr sites in the primitive cell of Cr_2O_3, which is induced by the ferromagnetic canting of spins along the $\boldsymbol{x}$ axis in three possible antiferromagnetic structures A1, A2, and A3. The directions of spins are denoted by the blue (dark) arrows. The directions of electronic polarization are denoted by the cyan (light) arrows. The Cr atoms are indicated by the big red spheres and the neighboring oxygen atoms are indicated by the small green spheres. The inversion center is indicated by $*$. The upper panel is the side view, while the lower panel is the top view. $\boldsymbol{a}$, $\boldsymbol{b}$, and $\boldsymbol{c}$ denote the directions of hexagonal lattice vectors, and $\boldsymbol{H}$ denotes the external magnetic field along $\boldsymbol{x}$ (in this setting, the angle between $\boldsymbol{a}$ and $\boldsymbol{b}$ is 120°, while $\boldsymbol{x}$ is perpendicular to $\boldsymbol{b}$ and $\boldsymbol{c}$). The notations $(\pm p^x, \pm p^y, 0)$ explain the symmetry properties of the induced polarization vectors $\partial \mathbf{P}/\partial e^x$ at four Cr sites. The numerical values of (p^x, p^y) are $(-0.08, 0.02)$, $(0.12, -0.57)$, and $(0.08, -0.79)\mu\mathrm{C\,m^{-2}}$ for A1, A2, and A3, respectively.

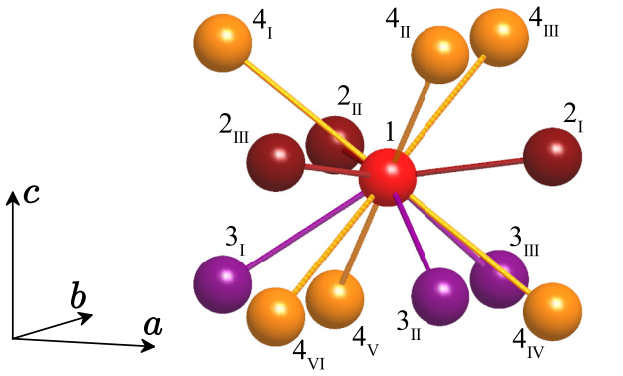

FIG. 3. Fragment of the crystal structure of Cr_2O_3: central Cr site of the type 1 and several coordinations spheres of the neighboring Cr sites of the types 2, 3, and 4. $\boldsymbol{a}$, $\boldsymbol{b}$, and $\boldsymbol{c}$ denote the directions of hexagonal lattice vectors.

constrained random-phase approximation (RPA) [33]. It can be further fitted in terms of two Kanamori parameters [34]: the intraorbital Coulomb repulsion $\mathcal{U} = 3.15$ eV and the exchange interaction $\mathcal{J} = 0.67$ eV. Then, the effective interaction responsible for the intraatomic exchange splitting between the minority- and majority-spin states can be evaluated as $U = \mathcal{U} + 2\mathcal{J}$ (~4.5 eV). The crystal-field splitting is about 100 meV [35]. Other parameters can be found elsewhere [36]. As we will see below, the model has serious limitations for the quantitative description of the ME effect in Cr_2O_3. Nevertheless, we consider it for the explanatory purposes.

The corundum structure of Cr_2O_3 has four interconnected Cr sublattices, which can be arranged antiferromagnetically as A1, A2, and A3 (see Fig. 2). Among them, the magnetic space group of A1 contains the spacial inversion $\hat{I}$ as it is, while in A2 and A3 $\hat{I}$ is combined with the time reversal $\hat{T}$. Thus the A1 structure allows for the weak ferromagnetism [2], while A2 and A3 are expected to exhibit the perpendicular ME effect, when the AFM structure is deformed by the external magnetic field [4] as explained in Fig. 2. The magnetic ground state of Cr_2O_3 is A3, which was also confirmed by our calculations of the total energies and parameters of isotropic exchange interactions. The directions of magnetic moments are parallel to $\boldsymbol{c} = z$.

Equations (8) and (10) allow us to rationalize the behavior of electronic polarization by separating the contributions of atomic pairs around each Cr site. Around site 1, the largest contributions to $\mathbf{P}$ comes from the atomic pairs in three coordinations spheres, formed by the atoms 2, 3, and 4, which are displayed in Fig. 3, and where the notations of atomic types is the same as in Fig. 2.

First, we note that the FM bond will not contribute to the perpendicular ME effect: even in the external field $\boldsymbol{H}$ such spins remain ferromagnetically aligned and, therefore, the cross product $[\boldsymbol{e}_i \times \boldsymbol{e}_j]$ will vanish. Moreover, in the case of perpendicular ME effect, the cross products $[\boldsymbol{e}_i \times \boldsymbol{e}_j]$ will be the same for all equivalent bonds.

Another important aspect is the symmetry. In order to estimate the ME coupling constant, we first evaluate the parameters $\boldsymbol{\mathcal{P}}_{ij}$, which obey the symmetry properties of the $R\bar{3}c$ group and contains all the information about the individual symmetry of the Cr_2O_3 lattice. For instance, the pseudovectors $\boldsymbol{\mathcal{P}}_{ij}$ in the nearest-neighbor (NN) bonds $\langle 13 \rangle$ and $\langle 24 \rangle$, parallel to the $\boldsymbol{c}$ axis (Fig. 2), will vanish due to the joint effect of threefold rotation and glade reflection, which transform this bond to itself. Then, for the bonds $\langle 12_\mathrm{I} \rangle$, $\langle 13_\mathrm{I} \rangle$, and $\langle 14_\mathrm{I} \rangle$, (see Fig. 3) the parameters $\boldsymbol{\mathcal{P}}_{ij}$ can be estimated (in $\mu\mathrm{C\,m^{-2}}$) as $(-0.066, 0.007, 0)$, $(0, 0.009, 0)$, and $(-0.002, 0.010, 0)$, respectively. The parameters for other bonds can be obtained from $\boldsymbol{\mathcal{P}}_{12_\mathrm{I}}$, $\boldsymbol{\mathcal{P}}_{13_\mathrm{I}}$, and $\boldsymbol{\mathcal{P}}_{14_\mathrm{I}}$ using the symmetry operations of the space group $R\bar{3}c$. Moreover, the threefold rotational about $\boldsymbol{c}$ yields the following property: $\sum_j \boldsymbol{\mathcal{P}}_{ij} = 0$. Nevertheless, the combination $\sum_j \boldsymbol{\epsilon}_{ji} \boldsymbol{\mathcal{P}}_{ij}$, which specifies the value of the electronic polarization (4), can be finite. All these properties do not depend on the type of the AFM order and will hold for A1, A2, and A3.

Then, we consider the behavior of the polarization vectors $\boldsymbol{p}_i = \sum_j \partial \boldsymbol{P}_{ij}/\partial e^x$, induced by the FM canting of spins along $\boldsymbol{x}$ (see Fig. 2). In the A1 phase, FM bonds between atoms 1 and 2 (3 and 4) will not contribute to $\boldsymbol{p}_i$. Thus one have to consider all possible connections of the sites 1 and 2 with the sites 3 and 4. Moreover, since the sites 1 and 2 (3 and 4) are transformed to each other by $\hat{I}$ (without flipping the spins), we will have: $\hat{I}\boldsymbol{\epsilon}_{ji}\boldsymbol{\mathcal{P}}_{ij} = -\boldsymbol{\epsilon}_{j'i'}\boldsymbol{\mathcal{P}}_{i'j'}$ but $[\boldsymbol{e}_i \times \boldsymbol{e}_j] = [\boldsymbol{e}_{i'} \times \boldsymbol{e}_{j'}]$, and, therefore, $\boldsymbol{p}_2 = -\boldsymbol{p}_1$ ($\boldsymbol{p}_4 = -\boldsymbol{p}_3$), where i' (j') is the inversion image of i (j). Thus, as expected [2,4], the FM canting of spins in the phase A1 will lead to the antiferroelectric behavior with no net

polarization. Our analysis provides a transparent microscopic explanation to it.

In the phases A2 and A3, however, the spins 1 and 2 (3 and 4) are coupled antiferromagnetically. Therefore these bonds will contribute to $\boldsymbol{p}_i$. Moreover, in addition to $\hat{I}\boldsymbol{\epsilon}_{ji}\boldsymbol{\mathcal{P}}_{ij} = -\boldsymbol{\epsilon}_{j'i'}\boldsymbol{\mathcal{P}}_{i'j'}$, the symmetry operation $\hat{I}\hat{T}$ will also flip the spins and, therefore, it will hold $[\boldsymbol{e}_i \times \boldsymbol{e}_j] = -[\boldsymbol{e}_{i'} \times \boldsymbol{e}_{j'}]$ and $\boldsymbol{p}_2 = \boldsymbol{p}_1$ ($\boldsymbol{p}_4 = \boldsymbol{p}_3$). That is why the FM canting of spins in A2 and A3 will result in the ME effect.

The direction of polarization, however, requires additional symmetry considerations, and this is the point where the direction of $\boldsymbol{H}$ comes into play. For instance, if (without field) all $\boldsymbol{e}_i$ are parallel to $\boldsymbol{z}$ and $\boldsymbol{H}$ is parallel to $\boldsymbol{x}$ (see Fig. 2), $[\boldsymbol{e}_i \times \boldsymbol{e}_j]$ will be parallel to $\boldsymbol{y}$ and, according to Eq. (4), we have to consider the behavior of $\mathcal{P}^y_{ij}$ and $\boldsymbol{\epsilon}_{ji}$ under the glade reflection $\{\hat{m}_y|\boldsymbol{c}/2\}$ ($\hat{m}_y$ being the mirror reflection $y \to -y$), connecting the sites 1 and 4 (2 and 3). In the A2 phase, this transformation is combined with $\hat{T}$ and, therefore, will additionally flip the spins. Then, it is straightforward to show (similar to above considerations for the effect of $\hat{I}$ and $\hat{I}\hat{T}$) that $\{\hat{m}_y|\boldsymbol{c}/2\}$ will lead to the additional symmetry properties: $p^x_1 = -p^x_4$ and $p^y_1 = p^y_4$ ($p^x_1 = p^x_4$ and $p^y_1 = -p^y_4$) for A2 (A3). This explains why **P** in A2 and A3 will be parallel to, respectively, $\boldsymbol{y}$ and $\boldsymbol{x}$.

The ME effect in Cr_2O_3 cannot be properly described by the phenomenological expression (2) [7,8]: in the case of ME effect, the cross product $[\boldsymbol{e}_i \times \boldsymbol{e}_j]$ is the same for all equivalent bonds. Then, the bonds $\langle 14_{\rm I}\rangle - \langle 14_{\rm VI}\rangle$ will not contribute to **P** because $\sum_j \boldsymbol{\epsilon}_{ji} = 0$ (see Fig. 3). For other types of bonds $\sum_j \boldsymbol{\epsilon}_{ji}$ can be finite and parallel to $\boldsymbol{z}$. Then, $\boldsymbol{H}||\boldsymbol{x}$ will yield $[\boldsymbol{e}_i \times \boldsymbol{e}_j]||\boldsymbol{y}$. Therefore, according to Eq. (2), the induced polarization should be always parallel to $\boldsymbol{x}$. This would explain the direction of polarization in A3, but not in A2.

Finally, we evaluate the matrix element of the ME tensor $\alpha_\perp$ at $T = 0$ (T being the temperature) using the numerical value of $p_x = 0.08\ \mu\mathrm{C\,m^{-2}}$ for the A3 phase and the chain rule: $\alpha_\perp \equiv \frac{\partial P^x}{\partial H^x} = \frac{\partial P^x}{\partial e^x}\frac{\partial e^x}{\partial H^x}$, where $\frac{\partial e^x}{\partial H^x}$ is estimated using parameters of the Heisenberg model $E_{\rm H} = -\sum_{i>j} J_{ij}\boldsymbol{e}_i \cdot \boldsymbol{e}_j$, obtained in the theory of infinitesimal spin rotations [23,37] as $\frac{\partial e^x}{\partial H^x} = -\frac{M}{J_0}$ ($M \approx 3\ \mu_{\rm B}$ being the spin magnetic moment and $J_0 = \sum_j J_{ij} \approx -116$ meV) [38]. It should be noted that the theory of infinitesimal spin rotations is the most suitable for treating small deformations of the magnetic system near the equilibrium, because it is more general and applicable even in the situations where the conventional SE theory breaks down. Nevertheless, when U is large and the orbital degrees of freedom are inactive (like for the half filling), the parameters J_{ij} are typically well consistent with results of the SE theory, given by Eq. (6) [23], as was also confirmed by present calculations. This again justifies the use of the SE theory. However, the obtained value of $\alpha_\perp \sim 2\times10^{-4}\ \mathrm{ps\,m^{-1}}$ is very small, which simply means that the considered spin-current effect is not the main mechanism of the ME coupling in Cr_2O_3. This is in line with modern understanding of the ME effect in Cr_2O_3, which is known include other contributions beyond the considered model. Particularly, the lattice effect is very important [26,27]. Moreover, the orbital magnetization, which is neglected in the considered half-filled t_{2g} model, can also contribute to $\alpha_\perp$ [26,28]. We expect that much better agreement with the experimental data can be achieved by considering a more general model, consisting of the Cr t_{2g} *and* e_g bands (see Fig. 1). For instance, we have found that the DM interactions are strongly underestimated in the t_{2g} only model in comparison with the five-orbital one. However, in the case of the five-orbital model, the $3d^3$ configuration does not longer correspond to the half filling, which will require some revision of Eq. (10) for the electric polarization. Below, we will consider several example of $3d^5$ compounds, which are described by the five orbital at the half filling, and argue that such model generally provides much better description for DM interactions and electronic polarization.

B. Linear magnetoelectric effect in $BiFeO_3$

$BiFeO_3$ is the well known type-I multiferroic, where the FE activity is manly related to the off-centrosymmetric atomic displacements of Bi and O, while magnetism originates from the half-filled $3d$ shell of Fe. The good aspect of $BiFeO_3$ is that the FE and AFM transition temperatures are high (1100 and 650 K, respectively), which makes it promising for practical applications [5]. In the bulk, the DM interactions, arising in the noncentrosymmetric $R3c$ structure, overcome the effect of magnetocrystalline anisotropy, thus, yielding the formation of incommensurate long-periodic spin-spiral texture [39–41]. Nevertheless, the magnetocrystalline anisotropy can be substantially increased in the thin films of $BiFeO_3$, leading to the formation of the G-type AFM phase. An interesting aspect of the G-phase is that it allows the possibility of having the linear ME effect, where the electric polarization rises linearly with the applied magnetic field, whereas in the incommensurate phase, this effect is averaged to zero by the spin-spiral modulation. The linear ME coupling α in the $BiFeO_3$ films was first experimentally studied in Ref. [42]. However, the obtained value of α was rather moderate (of the order of $0.51\ \mathrm{ps\,m^{-1}}$). The interest in this problem has reemerged again after the report of giant ME coupling, being of the order of $3\ \mathrm{V\,cm^{-1}\,Oe^{-1}}$ [43]. Even higher value of $24\ \mathrm{V\,cm^{-1}\,Oe^{-1}}$ (corresponding to $3\times10^4\ \mathrm{ps\,m^{-1}}$ [44]) was reported later in the composite films including $BiFeO_3$ [45].

In this section we will investigate the linear ME effect in $BiFeO_3$. The computational details and parameters of the model, constructed for the Fe $3d$ bands near the Fermi level, can be found in the previous publication [31].

The behavior of $\boldsymbol{\mathcal{P}}_{ij}$ can be understood on the cluster, where the central Fe site is surrounded by six nearest neighbors (Fig. 4). Other bonds can also produce a sizable contribution to the ME effect, though with some restrictions: for instance, all second NN bonds in the G-type AFM phase are ferromagnetic and, therefore, do not contribute to the ME effect (see discussions in Sec. III A). Using the model parameters, $\boldsymbol{\mathcal{P}}_{12_{\rm I}}$ corresponding to $\Delta\boldsymbol{\tau}_{2_{11}} = (-a, 0, \frac{c}{2})$ (where $a = 3.222$ Å and $c = 4.625$ Å are the rhombohedral lattice parameters), can be estimated as $\boldsymbol{\mathcal{P}}_{12_{\rm I}} = (7.88, -3.08, -1.68)\ \mu\mathrm{C\,m^{-2}}$. The parameters for other bonds can be obtained from $\boldsymbol{\mathcal{P}}_{12_{\rm I}}$ using the symmetry operations of the space group $R3c$, similar to the DM interactions considered in Ref. [31]. These parameters $\boldsymbol{\mathcal{P}}_{ij}$ are more than two orders of magnitude larger than

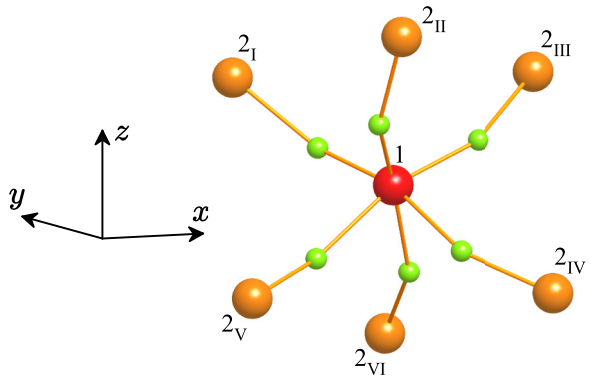

FIG. 4. Fragment of the crystal structure of $BiFeO_3$: central Fe site of the type 1 is surrounded by neighboring Fe sites of the type 2 (all are indicated by the big spheres). The intermediate O atoms are indicated by the small green spheres.

the ones obtained in the t_{2g} model for Cr_2O_3. Again, the threefold rotational about $\boldsymbol{z}$ imposes the symmetry constraint $\sum_j \mathcal{P}_{ij} = 0$. However, when $\mathcal{P}_{ij}$ in Eq. (4) is combined with $\boldsymbol{\epsilon}_{ji}$, one can expect finite $\boldsymbol{p}_i$.

In our analysis, we assume that the magnetocrystalline anisotropy confines the spins in the $\boldsymbol{xy}$ plane (the experimental situation). To be specific, we consider here only the case of $\boldsymbol{L}||\boldsymbol{y}$, where $\boldsymbol{L} = \frac{M}{2}(\boldsymbol{e}_1 - \boldsymbol{e}_2)$ is the AFM order parameter (Fig. 5). Due to the $R3c$ symmetry, similar analysis can be also applied for $\boldsymbol{L}||\boldsymbol{x}$. Then, we consider the effect of the magnetic field, which cants the spins in the direction of either $\boldsymbol{z}$ or $\boldsymbol{x}$.

In the first case ($\boldsymbol{H}||\boldsymbol{z}$), the active component of $\mathcal{P}_{ij}$, which is selected by $[\boldsymbol{e}_1 \times \boldsymbol{e}_2]$, is $\mathcal{P}^x_{ij}$. Then, by combing it with $\boldsymbol{\epsilon}_{ji}$, using the symmetry operation of the $R3c$ group, and noting that $\frac{\partial}{\partial e^z}[\boldsymbol{e}_1 \times \boldsymbol{e}_2] = 2$, it is straightforward to show that $p^x_1 \approx -16a\mathcal{P}^y_{12_I}/\sqrt{4a^2 + c^2}$, while $p^y_1 = p^z_1 = 0$. This NN contribution accounts for 65% of the total

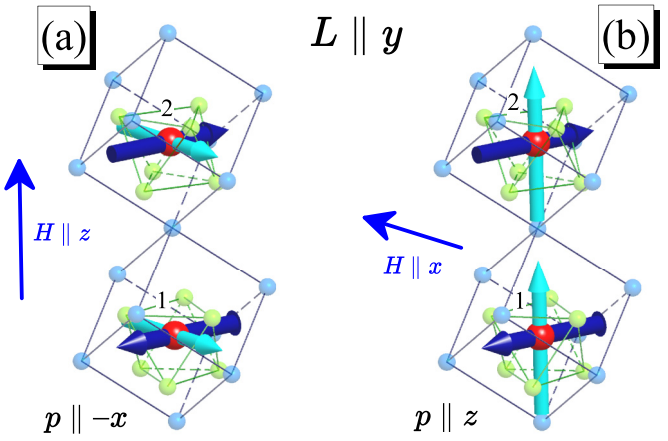

FIG. 5. Geometry of the linear magnetoelectric effect in $BiFeO_3$: the spin magnetic moments (denoted by dark blue arrows) are parallel to the $\boldsymbol{y}$ axis. Then, the external magnetic field applied along $\boldsymbol{z}$ ($\boldsymbol{x}$) induces the electric polarization along $-\boldsymbol{x}$ ($\boldsymbol{z}$), as illustrated in the part a (b). The Fe atoms are indicated by the big red spheres, the Bi atoms are indicated by the small blue spheres, and the O atoms are indicated by the small green spheres. The directions of polarization at each Fe site are denoted by light cyan arrows.

$p^x_1 = -78.2\ \mu\mathrm{C\,m^{-2}}$, obtained after summation of all bonds. Then, the symmetry operation $\{\hat{m}_y|(0,0,\frac{3c}{2})\}$, which transform the Fe sites 1 and 2 to each other, keeps the sign of ϵ^x, but changes the sign of $\mathcal{P}^x$ (as it holds for, respectively, normal vector and pseudovector). Moreover, in the G-type AFM phase, this transformation flips the spins. Altogether it leads to the property $p^x_2 = p^x_1$ and net electric polarization parallel to $\boldsymbol{x}$.

In the second case ($\boldsymbol{H}||\boldsymbol{x}$), the active component is $\mathcal{P}^z_{ij}$, yielding $p^x_1 = p^y_1 = 0$ and $p^z_1 \approx -12c\mathcal{P}^z_{12_I}/\sqrt{4a^2 + c^2}$ (note that in this case $\frac{\partial}{\partial e^x}[\boldsymbol{e}_1 \times \boldsymbol{e}_2] = -2$). The NN contribution accounts for 60% of the total $p^z_1 = 19.7\ \mu\mathrm{C\,m^{-2}}$. Similar to $\boldsymbol{H}||\boldsymbol{z}$, it is straightforward to show that $p^z_2 = p^z_1$, resulting in finite ME effect with the polarization parallel to $\boldsymbol{z}$.

The induced polarization satisfies the condition $\mathbf{P} \sim [\boldsymbol{H} \times \boldsymbol{L}]$, being in total agreement with results of the Ginzburg-Landau theory [46]. Finally, we evaluate matrix elements of the ME tensor, $\alpha_\parallel = \frac{\partial P^z}{\partial H^x}$ and $\alpha_\perp = \frac{\partial P^x}{\partial H^z}$ (for $\boldsymbol{L}||\boldsymbol{y}$), using the same procedure as for Cr_2O_3 and parameters of exchange interactions J_{ij} reported in Ref. [31], which are consistent with experimental data and reproduce the experimental value of Néel temperature (T_N). The SE theory, Eq. (6), yields similar parameters J_{ij}. Then, using the obtained value of $J_0 \approx -241$ meV and $M \approx 5\ \mu_B$, we will find $|\alpha_\parallel| = 0.03\ \mathrm{ps\,m^{-1}}$ and $|\alpha_\perp| = 0.12\ \mathrm{ps\,m^{-1}}$. These results are consistent (at least, by an order of magnitude) with direct calculations of electronic polarization for the model Hartree-Fock Hamiltonian without invoking the perturbation theory for the SO coupling, and also the experimental value of $0.51\ \mathrm{ps\,m^{-1}}$, reported in Ref. [42]. The giant enhancement of the ME coupling, which was reported in Refs. [43,45], probably requires additional mechanisms, such as the structural and magnetic reconstruction in the critical electric field, as was proposed in Refs. [46–48].

When the spins lie in the $\boldsymbol{xy}$ plane, there is also an "intrinsic ME effect" due to the FM canting of spins ($\sim 0.5^\circ$ [31,49]) in the direction perpendicular to $\boldsymbol{L}$, which is caused by DM interactions without any magnetic field. Below T_N, it leads to the polarization change ΔP^z, which can be estimated using the obtained values of $\mathcal{P}_{ij}$ as $0.2\ \mu\mathrm{C\,m^{-2}}$.

Below, we will critically examine the main approximations of our theory by considering the DM exchange interactions, which can be computed by using other techniques. First of all, the minimal model consisting only of the Fe $3d$ bands (and neglecting the contributions of O $2p$ bands) seems to be a good starting point for the analysis of magnetic properties of $BiFeO_3$ as it provides very reasonable estimates for T_N and the period of the spin-spiral texture in the bulk [31]. Parameters of DM interactions $\boldsymbol{d}_{12_I} = (0.106, -0.287, 0.140)$ meV, obtained in the SE theory for bare $\xi_0 = 53.1$ meV, agree reasonably well with $\boldsymbol{d}_{12_I} = (0.145, -0.418, 0.177)$ meV, derived using more general Green's function perturbation theory method for the same model [31]. Both superexchange and Green's function methods are the first-order theories with respect to the SO coupling. Nevertheless, the Green's function method does not employ additional approximations, such as the perturbation theory expansion with respect to the transfer integrals and the crystal field. The reasonable agreement obtained for the DM parameters demonstrates that such approximations are indeed justifiable. The conclusion is not obvious because the

t_{2g}-e_g level splitting in the octahedral environment is not small, being about 1.7 eV. Nevertheless, it is still smaller than the effective interaction $U \approx 5.8$ eV. Another important factor is the polarizability of the electron system by the SO interaction [31], which in our case is taken into account only approximately, by using the effective coupling $\xi = 123$ meV instead of ξ_0, where ξ was derived by fitting results of the SCLR calculations for matrix elements of the "screened" SO interactions with different projections spins. The "screened" SO interaction includes the bare contribution as well as all the self-consistent change of the Coulomb and exchange potential, treated on the mean-field level in the first order of the SO coupling. Thus the use of ξ instead of ξ_0 simply scales the DM parameter $\boldsymbol{d}_{12_1}$ by about factor of 2. Although it captures the main tendency, it deviates from $\boldsymbol{d}_{12_1} = (0.494, -1.450, 0.330)$ meV, obtained by combining SCLR with Green's function perturbation theory, which is the most rigorous method for the evaluation of DM interactions [31]. Thus our SE theory for the DM interactions and ME coupling is probably only semi-quantitative one. However, we believe that it should not change the main conclusions, particularly regarding the comparison with the experimental data for $BiFeO_3$.

Finally, we would also like to stress that the phenomenological expression (2) fails to describe the ME effect in $BiFeO_3$: for the canted spin structure, inherent to the ME effect, $[\boldsymbol{e}_i \times \boldsymbol{e}_j]$ is the same for all neighboring bonds surrounding each Fe site. By combining it with the symmetry property $\sum_j \boldsymbol{\epsilon}_{ji} = 0$, no ME effect would be expected if $\mathbf{P}_{ij} \propto \boldsymbol{\epsilon}_{ji} \times [\boldsymbol{e}_i \times \boldsymbol{e}_j]$, which is obviously not true.

C. Noncollinear spin order and ferroelectric polarization in $MnWO_4$

$MnWO_4$ has attracted a considerable attention as an example of the spin-spiral magnet, which was theoretically suggested to be a multiferroic [50]. This multiferroic behavior was indeed observed experimentally [50–52], and studied in many details after that [53–56]. Finite polarization was observed in the so-called noncollinear AF2 phase, which is realized in the temperature interval 7.6 K $< T <$ 12.5 K and described by the propagation vector $\mathbf{q}_{AF2} = (-0.214, \frac{1}{2}, 0.457)$ [51]. The spins rotate in the plane formed by the monoclinic $\boldsymbol{b}$ axis and one of the axes ($\boldsymbol{a}^*$) in the $\boldsymbol{ac}$ plane (see Fig. 6). The direction $\boldsymbol{a}^*$ is specified by the single-ion anisotropy. The electric polarization is parallel to the $\boldsymbol{b}$ axis, but can be realigned along $\boldsymbol{a}$ by applying the magnetic field parallel to $\boldsymbol{b}$. In the previous work [22] we have suggested that the FE activity in $MnWO_4$ may be related to the deformation of the spin-spiral texture, which explicitly breaks the inversion symmetry. The computational details and parameters of the effective low-energy model, constructed for the half-filled Mn3d bands of $MnWO_4$, can be also found in Ref. [22]. In this case, the effective interaction $U \sim 5$ eV is substantially larger than the Mn 3d bandwidth and the crystal-field splitting [22], so that the SE theory is applicable.

The direction of polarization in $MnWO_4$ is described by the phenomenological model (2). Indeed, for the spin rotation plane formed by $\boldsymbol{a}^*$ and $\boldsymbol{b}$, the cross product $[\boldsymbol{e}_i \times \boldsymbol{e}_j]$ is parallel to $\boldsymbol{c}^*$, which is another vector in the $\boldsymbol{ac}$ plane being perpendicular to $\boldsymbol{a}^*$. Then, for $\mathbf{q}_{AF2} = (-0.214, \frac{1}{2}, 0.457)$, there

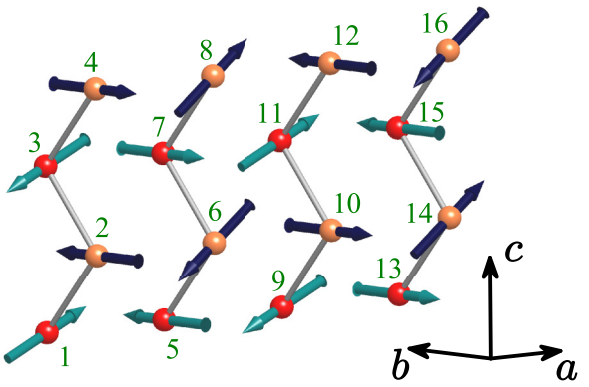

FIG. 6. Noncollinear spin-spiral texture with $\mathbf{q} = (-\frac{1}{4}, \frac{1}{2}, \frac{1}{2})$ in $MnWO_4$. $\boldsymbol{a}$, $\boldsymbol{b}$, and $\boldsymbol{c}$ are the monoclinic translation vectors. Two Mn sublattices, which are transformed to each other by the inversion operation, are indicated by red (dark) and orange (light) spheres.

are two types of noncollinear bonds for which $\boldsymbol{\epsilon}_{ji} || \boldsymbol{a}$ and $\boldsymbol{\epsilon}_{ji} || \boldsymbol{c}$. In both cases, the expression $\mathbf{P}_{ij} \propto \boldsymbol{\epsilon}_{ji} \times [\boldsymbol{e}_i \times \boldsymbol{e}_j]$ yields $\mathbf{P}_{ij} || \boldsymbol{b}$, which agrees with the experimental situation [51]. Nevertheless, below we will show that such agreement is rather fortuitous and the actual reason behind it is the specific $P2/c$ symmetry of $MnWO_4$.

The behavior of pseudovectors $\boldsymbol{\mathcal{P}}_{ij}$, reflecting these symmetry properties, is explained in Fig. 7. The parameters $\boldsymbol{\mathcal{P}}_{ij}$ are long-ranged and not restricted by the nearest neighbors. For instance, we have found sizable $\boldsymbol{\mathcal{P}}_{ij}$ spreading up to twelfth coordination sphere. Similar behavior was found for isotropic exchange interactions (being in total agreement with the experimental data [57]) and is related to the long-range character of the transfer integrals [22]. Due to the twofold rotation about $\boldsymbol{b}$ ($\hat{C}_b^2$), which is one of the symmetry operations of the $P2/c$ group (apart from a translation), in all equivalent bonds $\mathcal{P}^y$ will be the same, while $\mathcal{P}^x$ and $\mathcal{P}^z$ will change their signs. Moreover, if the bond connects two Mn sites of the same type (either I or II), $\hat{C}_b^2$ will transform it to the equivalent bond, separated by a translation. Therefore, for this type of bonds, we will have the additional condition $\mathcal{P}^x = \mathcal{P}^z = 0$. All these tendencies are clearly seen in Fig. 7.

Then, we consider the effect of noncollinear spin-spiral texture with $\mathbf{q} = (-\frac{1}{4}, \frac{1}{2}, \frac{1}{2})$ (Fig. 6), which is close to the experimental $\mathbf{q}_{AF2}$ [51]. First, we consider a perfect spiral texture. The effect of deformation of the spin spiral, which was proposed in Ref. [22], will be investigated after that.

The spin-spiral texture itself is stabilized by competing isotropic exchange interactions [22]. Nevertheless, its spacial orientation depends on the single-ion anisotropy and DM interactions, which also compete with each other: the former tends to align the spins in the $\boldsymbol{ac}$ plane (and cant them off the $\boldsymbol{a}$ axis by about 40°) [22,51]. However, the main DM vectors $\boldsymbol{d}_{ij}$ also lie in the $\boldsymbol{ac}$ plane ($\in \boldsymbol{ac}$) [22]. Thus, in order to minimize the energy of DM interactions, some of the spins should be parallel to the $\boldsymbol{b}$ axis ($||\boldsymbol{b}$), which conflicts with the single-ion anisotropy. Moreover, the DM exchange interactions compete with the isotropic ones. Thus the situation is indeed very subtle and the magnetic texture is rather fragile. Nevertheless, this is a very important point because, as we will see in a moment, the spacial orientation of the spin-spiral plane can control both magnitude *and* direction of the electric polarization.

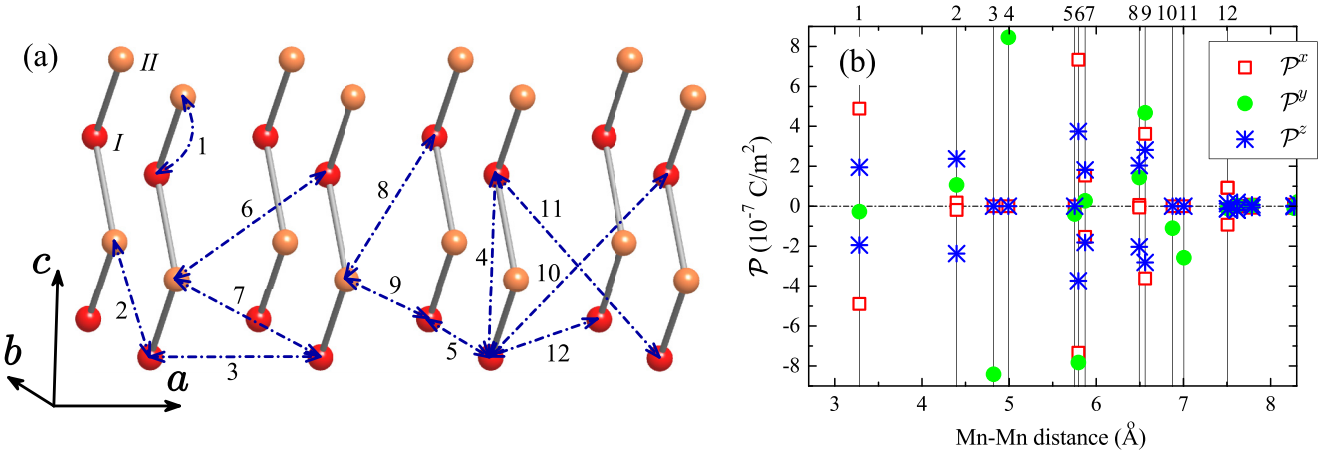

FIG. 7. (a) Fragment of the crystal structure of $MnWO_4$ with the explanation of the bond types surrounding Mn site I in twelve coordination spheres (other equivalent bonds are not shown). Two Mn sites in the primitive cell of $MnWO_4$ are denoted as I and II. $\boldsymbol{a}$, $\boldsymbol{b}$, and $\boldsymbol{c}$ are the monoclinic translation vectors. (b) Distance dependence of pseudovectors $\boldsymbol{\mathcal{P}} = (\mathcal{P}^x, \mathcal{P}^y, \mathcal{P}^z)$ (where $\boldsymbol{y} = \boldsymbol{b}$, $\boldsymbol{z} = \boldsymbol{c}$, and $\boldsymbol{x}$ is perpendicular to $\boldsymbol{y}$ and $\boldsymbol{z}$), specifying the electric polarization, in twelve coordination spheres (marked by vertical lines and numbered at the top). Due to the twofold rotational symmetry about $\boldsymbol{b}$, $\mathcal{P}^y$ in the equivalent bonds will be the same, while $\mathcal{P}^x$ and $\mathcal{P}^z$ will have opposite signs, as reflected in the figure.

First, we consider the experimental situation where the spin-spiral plane is formed by the $\boldsymbol{b}$ axis and one of directions $\boldsymbol{a}^*$ in the $\boldsymbol{ac}$ plane [51]. Then, considering the magnetic texture in Fig. 6, half of the spins is parallel to $\boldsymbol{b}$ and another half belongs to $\boldsymbol{ac}$. This means that for the bonds $\langle ij \rangle$ with unparallel spins, the cross-product $[\boldsymbol{e}_i \times \boldsymbol{e}_j]$ will also belong to $\boldsymbol{ac}$ and, therefore, the active components of $\boldsymbol{\mathcal{P}}_{ij}$ are $\mathcal{P}^x_{ij}$ and $\mathcal{P}^z_{ij}$. Then, for the equivalent bond $\langle i'j' \rangle$, which is obtained from $\langle ij \rangle$ by $\hat{C}_b^2$, we will have the following properties: $\mathcal{P}^x_{i'j'} = -\mathcal{P}^x_{ij}$, $\mathcal{P}^z_{i'j'} = -\mathcal{P}^z_{ij}$, and $[\boldsymbol{e}_{i'} \times \boldsymbol{e}_{j'}] = -[\boldsymbol{e}_i \times \boldsymbol{e}_j]$. The latter property holds because $\hat{C}_b^2$ reverses the direction of propagation of the spin-spiral along $\boldsymbol{a}$ and $\boldsymbol{c}$. Therefore, if the bond $\langle ij \rangle$ is along the propagation direction, the bond $\langle i'j' \rangle$ lies in the opposite direction. Thus, according to Eq. (4), the finite polarization is possible in the direction, which does not change under $\hat{C}_b^2$ (and keeps the sign of corresponding components of the vectors $\boldsymbol{\epsilon}_{ji}$). For the considered geometry of the spin spiral, this direction is $\boldsymbol{b}$, being in total agreement with the experimental data [51]. However, the absolute value of the polarization depends on the orientation of spins in the $\boldsymbol{ac}$ plane. Indeed, according to Eq. (4), if $\boldsymbol{e}_i = (0,1,0)$ and $\boldsymbol{e}_j = (\sin\beta, 0, \cos\beta)$, the polarization behaves as $P^y_{ij} \sim (\mathcal{P}^x_{ij} \cos\beta - \mathcal{P}^z_{ij} \sin\beta)$. The dependence of total polarization $P^y = \sum_j P^y_{ij}$ on β, obtained using the numerical values of $\mathcal{P}^x_{ij}$ and $\mathcal{P}^z_{ij}$, is displayed in Fig. 8. Thus one can conclude the follows. (i) The finite polarization in $MnWO_4$ can be indeed induced by the spiral magnetic order. In this sense, the conclusion of our previous work [22] about crucial importance of inhomogeneity (or deformation) of the spin-spiral order was exaggerated. (ii) The absolute value of P^y strongly depends on the orientation of spins in the $\boldsymbol{ac}$ plane. The maximal value of about 25 μC m^{-2} is comparable with experimental 50 μC m^{-2} [51]. However, it does not mean that this maximal value is realized for the same β, which minimizes the total energy of the system. The directions of spins are controlled by anisotropic interactions, which are small in $MnWO_4$ [22]. Therefore the situation is very fragile. This probably explains the large spread of P^y reported in electronic structure calculations, which are typically underestimated in comparison with the experimental data [22,58,59].

Then, we consider the situation when all spins lie in the $\boldsymbol{ac}$ plane and also form the spin-spiral texture with the propagation vector $\mathbf{q} = (-\frac{1}{4}, \frac{1}{2}, \frac{1}{2})$. This behavior was observed experimentally in the magnetic filed $\boldsymbol{H}||\boldsymbol{b}$, which causes the spin-flop-like transition and orients the spins in the $\boldsymbol{ac}$ plane, also changing the direction of experimental polarization from $\mathbf{P}||\boldsymbol{b}$ to mainly $\mathbf{P}||\boldsymbol{a}$ [51]. In this case, $[\boldsymbol{e}_i \times \boldsymbol{e}_j]$ is parallel to $\boldsymbol{b}$ and the active component of $\boldsymbol{\mathcal{P}}_{ij}$ is $\mathcal{P}^y_{ij}$. Then, for two bonds $\langle ij \rangle$ and $\langle i'j' \rangle$, which are transformed to each other by $\hat{C}_b^2$, we will have: $\mathcal{P}^y_{i'j'} = \mathcal{P}^y_{ij}$ and $[\boldsymbol{e}_{i'} \times \boldsymbol{e}_{j'}] = -[\boldsymbol{e}_i \times \boldsymbol{e}_j]$. Therefore the finite polarization is possible in the directions $\boldsymbol{a}$ and $\boldsymbol{c}$, which are reversed by $\hat{C}_b^2$. The direction of polarization in the plane $\boldsymbol{ac}$ is not specified by the symmetry. Using the numerical values of $\mathcal{P}^y_{ij}$ (Fig. 7), we obtain $P^x = 36.6$ μC m^{-2} and $P^z = 9.4$ μC m^{-2}. In agreement to the symmetry arguments [55], our theory also predicts small polarization along

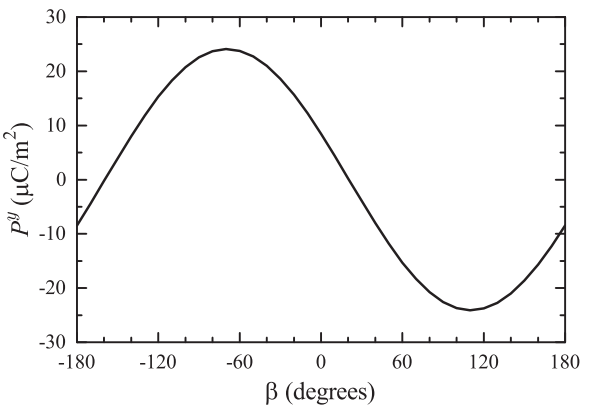

FIG. 8. Electric polarization P^y of the spin-spiral phase of $MnWO_4$ with $\mathbf{q} = (-\frac{1}{4}, \frac{1}{2}, \frac{1}{2})$, where half of the spins are parallel to the $\boldsymbol{b}$ axis, while another half lies in the $\boldsymbol{ac}$ plane and forms the angle β with the monoclinic $\boldsymbol{c}$ axis (see Fig. 6).

$\boldsymbol{c}$, which could be verified experimentally. This conclusion is formally consistent with the phenomenological model (2). Nevertheless, we would like to emphasize that the actual reason for such behavior, both for $\mathbf{P}||\boldsymbol{b}$ and $\mathbf{P} \in \boldsymbol{ac}$, is the specific symmetry of $MnWO_4$ and the existence of the twofold rotation $\hat{C}_b^2$ among symmetry operations of the space group $P2/c$.

Finally, we discuss the effect of spin-spiral inhomogeneity on the electronic polarization P^y in the ground state [22]. This inhomogeneity is caused by the competition of isotropic and DM exchange interactions, which breaks the inversion symmetry and makes two Mn sublattices inequivalent (see Fig. 6 for the notations). Particularly, for the $\mathbf{q} = (-\frac{1}{4}, \frac{1}{2}, \frac{1}{2})$ texture, half of the spins will remain parallel to the $\boldsymbol{b}$ axis, while another half will split in two groups, forming different angles β with respect to the $\boldsymbol{c}$ axis (69° and 56°, respectively) [22]. Then, the Mn sites 1, 2, 5 and 6 in Fig. 6 (and equivalent to them sites) will have different magnetic environment, which will result in four distinct values of $\mathbf{P}_i = \sum_j \mathbf{P}_{ij}$, respectively: 25.3, 20.0, 11.8, and 21.2 μC m^{-2}. The total polarization in this case is the average value of these four, yielding 19.6 μC m^{-2}, which is consistent with the value of electric polarization $|\mathbf{P}| \sim 16\,\mu$C m^{-2} of homogeneous spin-spiral with the average $\beta = 61.5°$ (see Fig. 8). Thus the spin-spiral deformation in $MnWO_4$ does not seem to make the main contribution to $\mathbf{P}$, contrary to the manganites, where the deformation is substantially larger and contributes to the polarization via the nonrelativistic double exchange mechanism [18].

D. Symmetry constraints on the direction of polarization in spin-spiral MnO_2

The rutile (β-) phase of MnO_2 is another interesting example. Due to competing first- and second-neighbor AFM exchange interactions, it develops the incommensurate spin-spiral order below $T_N \approx 92$ K [60,61]. The spin spiral propagates along the tetragonal $\boldsymbol{c}$ axis ($= z$). Therefore, from the viewpoint of spin-current theory, it could be another potentially multiferroic compound [7,8], although it has never been considered in this context. In this section, we will show that the multiferroic effect can be indeed expected in the rutile phase of MnO_2. Moreover, the behavior of electronic polarization obeys the phenomenological rule $\mathbf{P} \propto \boldsymbol{c} \times [\boldsymbol{e}_i \times \boldsymbol{e}_j]$ [7,8]. Nevertheless, we will argue that the actual reason behind it is related to the specific $P4_2/mnm$ symmetry of MnO_2, which imposes the symmetry constraints on the properties of $\boldsymbol{\mathcal{P}}_{ij}$.

We use the experimental parameters of the crystal structure, reported in Ref. [62]. There are two Mn sites in the primitive cell, which are connected by the symmetry operations of the space group $P4_2/mnm$. Like in Cr_2O_3, we consider the minimal model comprising of half-filled t_{2g} bands near the Fermi level (Fig. 9). In this case, the crystal-field splitting of t_{2g} levels is pretty large (about 370 meV). The Kanamori parameters of screened intraorbital Coulomb and exchange interactions are 3.0 and 0.72 eV, respectively. Other parameters can be found elsewhere [36]. According to the theory of infinitesimal spin rotations [37], the isotropic exchange interactions between first and second neighbors, located at $(0,0,\pm c)$ and $(\pm\frac{a}{2}, \pm\frac{a}{2}, \pm\frac{c}{2})$ (a and c being the tetragonal lattice parameters), are -16.4 and -12.3 meV, respectively. Similar parameters are obtained

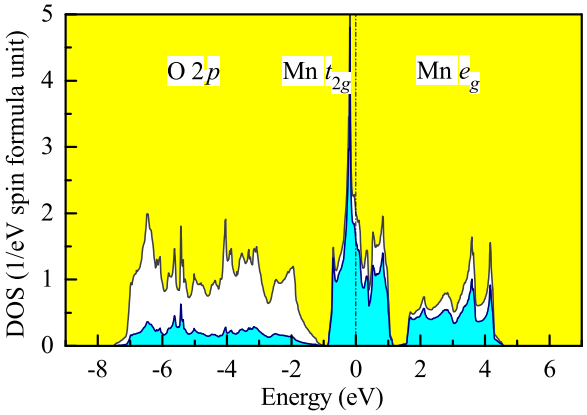

FIG. 9. Total and partial densities of states of MnO_2 in the local density approximation. The shaded light (blue) area shows contributions of the Mn $3d$ states. Positions of the main bands are indicated by symbols. The Fermi level is at zero energy (shown by dot-dashed line).

in the frameworks of the SE theory, Eq. (6). These exchange interactions support the appearance of spin-spiral superstructure with $\mathbf{q} \approx (0,0,\frac{1}{7})$ (comprising of seven primitive cells), in agreement with the experimental data [60] and results of first-principle calculations [63]. Moreover, the magnetocrystalline anisotropy energy confines the spins in the $\boldsymbol{xy}$ plane.

The $P4_2/mnm$ space group imposes the symmetry constrains on the properties of $\boldsymbol{\mathcal{P}}_{ij}$, which are explained in Fig. 10. The parameters $\boldsymbol{\mathcal{P}}_{ij}$ in the NN bonds $(0,0,\pm c)$ vanish identically due to the mmm symmetry. Then, due to the symmetry operations $\{\hat{C}_c^4|(\frac{a}{2},\frac{a}{2},\frac{c}{2})\}$ and $\{\hat{m}_x|(\frac{a}{2},\frac{a}{2},\frac{c}{2})\}$ ($\hat{C}_c^4$ being the fourfold rotation about $\boldsymbol{c}$), transforming the second-neighbor bonds to themselves, the corresponding parameters will behave as $\boldsymbol{\mathcal{P}}_{ij} = (\pm\mathcal{P}, \pm\mathcal{P}, 0)$ (see Fig. 10). Therefore it is straightforward to see that the spin spiral, propagating along $\boldsymbol{c}$ ($= z$) and rotating in the $\boldsymbol{xy}$ plane, does not induce any polarization because the active component $\mathcal{P}_{ij}^z$ is identically equals to zero. For other bonds with lower symmetry, some of $\mathcal{P}_{ij}^z$ can be finite. However, the phases of $\boldsymbol{\epsilon}_{ji}\mathcal{P}_{ij}^z$ alternate for the equivalent types of bonds, again resulting in no net polarization.

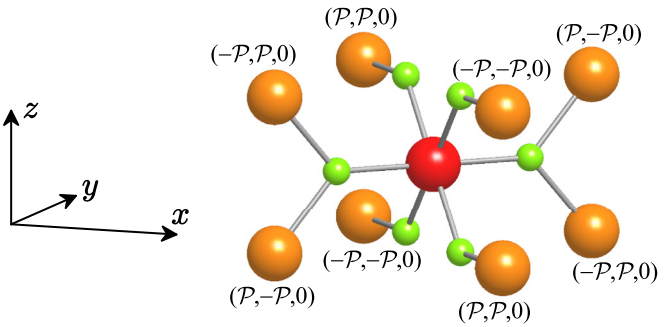

FIG. 10. Fragment of the crystal structure of MnO_2 illustrating the symmetry properties of pseudovectors $\boldsymbol{\mathcal{P}}_{ij}$ in eight neighboring bonds, connecting two types of Mn sites. The Mn atoms are indicated by the big spheres and the O atoms are indicated by the small spheres. The numerical value of parameter $\mathcal{P}$ is 0.023 μC m^{-2}.

However, when the spins rotate in the yz, the active component is $\mathcal{P}^x_{ij}$, which is finite. Moreover, by combining the phases of $\mathcal{P}^x_{ij}$ with the ones of $\boldsymbol{\epsilon}_{ji}$, it is straightforward to see that $P^x = P^z = 0$, while P^y can be finite. Using obtained parameters $\mathcal{P}^x_{ij}$, P^y for $\mathbf{q} \approx (0,0,\frac{1}{7})$ can be estimated as 2 μC cm^{-2}. Similar conclusion holds when the spins rotate in the zx plane.

Thus we expect no FE activity in the magnetic ground state of MnO_2. However, small polarization can be induced by aligning the spins in either yz or zx plane. This can be done by applying the external magnetic field along either x or y axis. Thus our finding can be verified experimentally. The result is formally consistent with the phenomenological expression $\mathbf{P} \propto \boldsymbol{c} \times [\boldsymbol{e}_i \times \boldsymbol{e}_j]$ [7,8]. However, it should be understood that the actual reason behind it is again the specific symmetry of the rutile phase of MnO_2.

E. Symmetry aspects of the electric polarization in $CuFeO_2$ and MnI_2

The triangular-lattice compounds such as $CuFeO_2$ and MnI_2 (crystallizing in the space groups $R\bar{3}m$ and $P\bar{3}m1$, respectively) have attracted a considerable attention as examples of proper-screw spin-spiral multiferroics where the phenomenological KNB theory breaks down. Experimentally, the direction of propagation of the spin-spiral $\mathbf{q}$ can be controlled by the magnetic field. However, for all magnetic configurations, $\mathbf{q}$ is perpendicular to the spin rotation plane and, therefore, according to Eq. (2), there should be no electric polarization. Nevertheless, the experimental measurements revealed finite polarization [10,11,64], which was also confirmed by first-principles calculations [16].

The Mn (Fe) atoms in MnI_2 ($CuFeO_2$) form the triangular plane, which is explained in Fig. 11. Then, the experimental finding can be summarized as follows [11]: for $\mathbf{q}||\boldsymbol{x}$ or $\boldsymbol{y}$, the electric polarization is parallel to $\boldsymbol{y}$. In this section we will show that this result can be easily rationalized by using new Eq. (4).

Due to the inversion and threefold rotation symmetries, the coordinates of six normal vectors $\boldsymbol{\epsilon}_{j0}$ around each TM site are given by $\boldsymbol{\epsilon}_{j0} = (\sin\frac{\pi j}{3}, \cos\frac{\pi j}{3}, 0)$, while corresponding pseudovectors $\boldsymbol{\mathcal{P}}_{0j}$ are transformed as $\boldsymbol{\mathcal{P}}_{0j} = (-1)^j(\sin\frac{\pi j}{3}, \cos\frac{\pi j}{3}, 0)\mathcal{P}$ (see Fig. 11 for the notation of atomic positions). Then, for $\mathbf{q}||\boldsymbol{x}$, the spins rotate in the yz plane relative to $\boldsymbol{e}_0 = (0,0,1)$ as $\boldsymbol{e}_j = (0, -\sin(\epsilon^x_{j0}aq), \cos(\epsilon^x_{j0}aq))$, where a is the lattice parameter. Therefore the active component of $\boldsymbol{\mathcal{P}}_{0j}$ is x, and after summing up the contributions from all six neighbors we will obtain that $\mathbf{P} = (0, P^y, 0)$ and $P^y = -\sqrt{3}\mathcal{P}\sin(\frac{\sqrt{3}}{2}aq)$. Very similary, if $\mathbf{q}||\boldsymbol{y}$, the spins rotate in the zx plane as $\boldsymbol{e}_j = (\sin(\epsilon^y_{j0}aq), 0, \cos(\epsilon^y_{j0}aq))$. Then, the active component of $\boldsymbol{\mathcal{P}}_{0j}$ is y, and the total polarization is again parallel to $\boldsymbol{y}$, where $P^y = \mathcal{P}\sin(\frac{1}{2}aq)(4\cos(\frac{1}{2}aq) - 1)$.

Thus the symmetry properties of the electric polarization in the triangular-lattice compounds are naturally reproduced by Eq. (4). The numerical estimates for MnI_2, obtained by fitting results of first-principles calculations to Moriya's expression (1), can be found in Ref. [16].

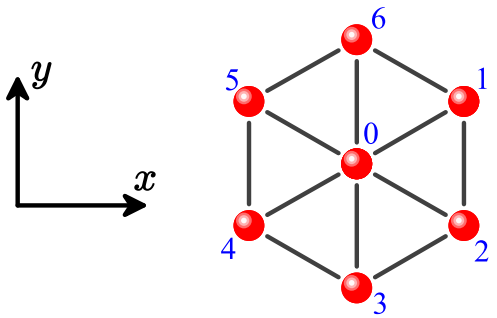

FIG. 11. Atoms of Mn (Fe) in the triangular lattice of MnI_2 ($CuFeO_2$).

IV. SUMMARY AND CONCLUSIONS

We have derived an analytical expression for the electronic polarization driven by the SO interaction in noncollinear magnets. For these purposes, we have considered the Berry-phase theory of electric polarization and applied it to the Hubbard model at the half filling. Thus our analysis is limited by the spin-current mechanism and does not involve additional complications caused by lattice distortions and orbital degrees of freedom. Moreover, all derivations are performed in the spirit of the SE theory, which is valid in the first order of the SO coupling and in the lowest order of $\hat{t}_{ij}/U$, similar to the analysis of DM exchange interactions [3].

We have found that the electric polarization in each bond is given by Eq. (4), which represents a substantial revision of the phenomenological expression (2). Namely, the electronic polarization in Eq. (4) explicitly depends on the symmetry of the lattice (similar to the DM exchange interactions $\boldsymbol{d}_{ij}$ [2]): this dependence is described by the pseudovector $\boldsymbol{\mathcal{P}}_{ij}$, which is coupled to the cross product $[\boldsymbol{e}_i \times \boldsymbol{e}_j]$, depending on the directions of spins. Thus this coupling describes how the symmetry of the lattice interferes with the symmetry of the noncollinear arrangement of spins. The direction of the polarization itself is specified by the unit vectors $\boldsymbol{\epsilon}_{ji}$, describing the spacial orientation of the magnetic bonds, which are modulated by the scalar $\boldsymbol{\mathcal{P}}_{ij} \cdot [\boldsymbol{e}_i \times \boldsymbol{e}_j]$. We have argued that, even though the direction of polarization in some spin-spiral magnets can be described by the phenomenological expression (2), the actual reason behind it is the specific symmetry of the considered system, which are described by the pseudovectors $\boldsymbol{\mathcal{P}}_{ij}$. Moreover, we have shown that the spin-current mechanism is much more generic and operates not only in spin-spiral compounds, but also in other types of noncollinear magnets, where the phenomenological expression (2) breaks down. Particularly, absolutely the same mechanism may lead to the ME effect induced by the FM canting of spins in magnetic field. Furthermore, the new expression (4) naturally explains the symmetry properties of the electric polarization in spin-spiral magnets with triangular lattice.

Another important factor, which plays a crucial role, even at the half filling, is the crystal-field splitting. We have shown that without the crystal field, both DM exchange interactions and electronic polarization would vanish. However, the crystal field may have other interesting consequences. For instance, it leads to the asphericity in the distribution of the charge density around each transition-metal site and, if the latter is located

not in the centrosymmetric position, one can also expect ionic contribution to the electronic polarization, which can be also derived from the Berry-phase theory, as was demonstrated recently for $Ba_2CoGe_2O_7$ [12]. This is also consistent with the phenomenological analysis by Moriya [6], who expressed the total polarization as the sum of ionic contributions and the ones originating from the bonds. The ionic contributions were also evaluated in the present work but found to be at least one order of magnitude smaller than the "anomalous" pair contributions, which are given by Eq. (4) and related to fine details of the electronic structure [65].

Using parameters of the effective Hubbard model, derived from the first-principles electronic structure calculations, we have evaluated the spin-current contribution to the electronic polarization for the series of ME materials (Cr_2O_3 and $BiFeO_3$) and multiferroics compounds with the spin-spiral structure ($MnWO_4$ and MnO_2). We have shown that, although Eq. (4) excellently reproduces the symmetry properties of the polarization, its numerical values can be severely underestimated, depending on the material. Particularly, the largest discrepancy was found for the ME effect in Cr_2O_3, which suggest the importance of other (lattice and orbital) contributions, in agreement with the previous finding [26–28].

We have also clarified the microscopic origin of FE activity in the spin-spiral phase of $MnWO_4$: although in this case the spin spiral is deformed by competing isotropic and antisymmetric DM exchange interactions, which explicitly breaks the inversion symmetry [22], this deformation seems to have a secondary effect on the value of electronic polarization. The main contribution comes from the spin-current mechanism, given by Eq. (4), which also describes the change of the direction of polarization, depending on the spacial orientation of the spin spiral. Finally, we have predicted the FE activity in the rutile phase of MnO_2—yet another spin-spiral magnet, where a finite polarization can be obtained by rotating the spins out of the tetragonal $\boldsymbol{x}\,\boldsymbol{y}$ plane.

[1] A. Manchon, H. C. Koo, J. Nitta, S. M. Frolov, and R. A. Duine, Nat. Mater. **14**, 871 (2015); F. Cardano and L. Marrucci, Nat. Photon. **9**, 776 (2015); K. Y. Bliokh, F. J. Rodríguez-Fortuño, F. Nori, and A. V. Zayats, *ibid.* **9**, 796 (2015); E. I. Rashba, J. Phys.: Condens. Matter **28**, 421004 (2016).

[2] I. Dzyaloshinsky, J. Chem. Phys. Solids **4**, 241 (1958).

[3] T. Moriya, Phys. Rev. **120**, 91 (1960).

[4] I. E. Dzyaloshinskii, Zh. Eksp. Teor. Fiz. **37**, 881 (1960) [JETP (USSR) **10**, 628 (1960)].

[5] T. Kimura, Annu. Rev. Mater. Res. **37**, 387 (2007); S.-W. Cheong and M. Mostovoy, Nat. Mater. **6**, 13 (2007); D. Khomskii, Physics **2**, 20 (2009); Y. Tokura and S. Seki, Adv. Mater. **22**, 1554 (2010).

[6] T. Moriya, J. Appl. Phys. **39**, 1042 (1968).

[7] H. Katsura, N. Nagaosa, and A. V. Balatsky, Phys. Rev. Lett. **95**, 057205 (2005).

[8] M. Mostovoy, Phys. Rev. Lett. **96**, 067601 (2006).

[9] I. A. Sergienko and E. Dagotto, Phys. Rev. B **73**, 094434 (2006).

[10] T. Arima, J. Phys. Soc. Jpn. **76**, 073702 (2007).

[11] T. Kurumaji, S. Seki, S. Ishiwata, H. Murakawa, Y. Tokunaga, Y. Kaneko, and Y. Tokura, Phys. Rev. Lett. **106**, 167206 (2011).

[12] I. V. Solovyev, Phys. Rev. B **91**, 224423 (2015).

[13] R. D. King-Smith and D. Vanderbilt, Phys. Rev. B **47**, 1651(R) (1993); D. Vanderbilt and R. D. King-Smith, *ibid.* **48**, 4442 (1993).

[14] R. Resta, J. Phys.: Condens. Matter **22**, 123201 (2010).

[15] N. Marzari, A. A. Mostofi, J. R. Yates, I. Souza, and D. Vanderbilt, Rev. Mod. Phys. **84**, 1419 (2012).

[16] H. J. Xiang, E. J. Kan, Y. Zhang, M.-H. Whangbo, and X. G. Gong, Phys. Rev. Lett. **107**, 157202 (2011).

[17] P. Barone, K. Yamauchi, and S. Picozzi, Phys. Rev. Lett. **106**, 077201 (2011).

[18] I. V. Solovyev and S. A. Nikolaev, Phys. Rev. B **87**, 144424 (2013); **90**, 184425 (2014).

[19] K. Yamauchi and P. Barone, J. Phys.: Condens. Matter **26**, 103201 (2014).

[20] I. V. Solovyev, Phys. Rev. B **83**, 054404 (2011); **90**, 179910(E) (2014).

[21] W. C. Koehler, J. W. Cable, M. K. Wilkinson, and E. O. Wollan, Phys. Rev. **151**, 414 (1966); G. P. Felcher, G. H. Lander, T. Arai, S. K. Sinha, and F. H. Spedding, Phys. Rev. B **13**, 3034 (1976).

[22] I. V. Solovyev, Phys. Rev. B **87**, 144403 (2013).

[23] I. V. Solovyev, J. Phys.: Condens. Matter **20**, 293201 (2008).

[24] P. W. Anderson, Phys. Rev. **115**, 2 (1959).

[25] A. Malashevich and D. Vanderbilt, Phys. Rev. Lett. **101**, 037210 (2008); Phys. Rev. B **80**, 224407 (2009).

[26] A. Malashevich, S. Coh, I. Souza, and D. Vanderbilt, Phys. Rev. B **86**, 094430 (2012).

[27] E. Bousquet, N. A. Spaldin, and K. T. Delaney, Phys. Rev. Lett. **106**, 107202 (2011).

[28] A. Scaramucci, E. Bousquet, M. Fechner, M. Mostovoy, and N. A. Spaldin, Phys. Rev. Lett. **109**, 197203 (2012).

[29] See Supplemental Material at http://link.aps.org/supplemental/10.1103/PhysRevB.95.214406 for details of derivations of parameters of DM interactions and electronic polarization in the framework of the SE theory.

[30] O. K. Andersen, Phys. Rev. B **12**, 3060 (1975).

[31] I. V. Solovyev, Phys. Rev. B **90**, 024417 (2014).

[32] We use the experimental lattice parameters, reported by P. J. Brown, J. B. Forsyth, E. Lelièvre-Berna, and F. Tasset, J. Phys.: Condens. Matter **14**, 1957 (2002).

[33] F. Aryasetiawan, M. Imada, A. Georges, G. Kotliar, S. Biermann, and A. I. Lichtenstein, Phys. Rev. B **70**, 195104 (2004).

[34] J. Kanamori, Prog. Theor. Phys. **30**, 275 (1963).

[35] I. V. Solovyev, Phys. Rev. B **73**, 155117 (2006).

[36] All model parameters are available upon request.

[37] A. I. Liechtenstein, M. I. Katsnelson, V. P. Antropov, and V. A. Gubanov, J. Magn. Magn. Mater. **67**, 65 (1987).

[38] The corresponding Néel temperature, estimated in the framework of Tyablikov's RPA [S. V. Tyablikov, *Methods of Quantum Theory of Magnetism* (Nauka, Moscow, 1975)] using the obtained parameters J_{ij} for Cr_2O_3, is $T_N = 250$ K, which is in fair agreement with the experimental value of 308 K [E. J. Samuelsen, M. T. Hutchings, and G. Shirane, Physica **48**, 13 (1970)].

[39] I. Sosnowska and A. K. Zvezdin, J. Magn. Magn. Matter. **140–144**, 167 (1995).
[40] J. Jeong, E. A. Goremychkin, T. Guidi, K. Nakajima, G. S. Jeon, S.-A. Kim, S. Furukawa, Y. B. Kim, S. Lee, V. Kiryukhin, S. W. Cheong, and J.-G. Park, Phys. Rev. Lett. **108**, 077202 (2012).
[41] M. Matsuda, R. S. Fishman, T. Hong, C. H. Lee, T. Ushiyama, Y. Yanagisawa, Y. Tomioka, and T. Ito, Phys. Rev. Lett. **109**, 067205 (2012).
[42] J.-P. Rivera and H. Schmid, Ferroelectrics **204**, 23 (1997).
[43] J. Wang, J. B. Neaton, H. Zheng, V. Nagarajan, S. B. Ogale, B. Liu, D. Viehland, V. Vaithyanathan, D. G. Schlom, U. V. Waghmare, N. A. Spaldin, K. M. Rabe, M. Wuttig, and R. Ramesh, Science **299**, 1719 (2003).
[44] T. Stevenson, J. Bennett, A. P. Brown, T. Wines, A. J. Bell, R. I. Smith, and T. P. Comyn, APL Mater. **2**, 086105 (2014).
[45] M. Lorenz, G. Wagner, V. Lazenka, P. Schwinkendorf, H. Modarresi, M. J. Van Bael, A. Vantomme, K. Temst, O. Oeckler, and M. Grundmann, Appl. Phys. Lett. **106**, 012905 (2015).
[46] A. F. Popkov, M. D. Davydova, K. A. Zvezdin, S. V. Solov'yov, and A. K. Zvezdin, Phys. Rev. B **93**, 094435 (2016).
[47] S. Lisenkov, I. A. Kornev, and L. Bellaiche, Phys. Rev. B **79**, 012101 (2009).
[48] N. E. Kulagin, A. F. Popkov, S. V. Solov'ev, K. S. Sukmanova, and A. K. Zvezdin, Phys. Solid State **57**, 933 (2015).
[49] C. Ederer and N. A. Spaldin, Phys. Rev. B **71**, 060401(R) (2005).
[50] O. Heyer, N. Hollmann, I. Klassen, S. Jodlauk, L. Bohatý, P. Becker, J. A. Mydosh, T. Lorenz, and D. Khomskii, J. Phys.: Condens. Matter **18**, L471 (2006).
[51] K. Taniguchi, N. Abe, T. Takenobu, Y. Iwasa, and T. Arima, Phys. Rev. Lett. **97**, 097203 (2006).
[52] A. H. Arkenbout, T. T. M. Palstra, T. Siegrist, and T. Kimura, Phys. Rev. B **74**, 184431 (2006).
[53] H. Mitamura, T. Sakakibara, H. Nakamura, T. Kimura, and K. Kindo, J. Phys. Soc. Jpn. **81**, 054705 (2012).
[54] I. Urcelay-Olabarria, E. Ressouche, A. A. Mukhin, V. Yu. Ivanov, A. M. Kadomtseva, Yu. F. Popov, G. P. Vorobev, A. M. Balbashov, J. L. García-Muñoz, and V. Skumryev, Phys. Rev. B **90**, 024408 (2014).
[55] I. Urcelay-Olabarria, J. L. García-Muñoz, and A. A. Mukhin, Phys. Rev. B **91**, 104429 (2015).
[56] Y. Xiao, C. M. N. Kumar, S. Nandi, Y. Su, W. T. Jin, Z. Fu, E. Faulhaber, A. Schneidewind, and Th. Brückel, Phys. Rev. B **93**, 214428 (2016).
[57] F. Ye, R. S. Fishman, J. A. Fernandez-Baca, A. A. Podlesnyak, G. Ehlers, H. A. Mook, Y. Wang, B. Lorenz, and C. W. Chu, Phys. Rev. B **83**, 140401(R) (2011).
[58] C. Tian, C. Lee, H. Xiang, Y. Zhang, C. Payen, S. Jobic, and M.-H. Whangbo, Phys. Rev. B **80**, 104426 (2009).
[59] K. V. Shanavas, D. Choudhury, I. Dasgupta, S. M. Sharma, and D. D. Sarma, Phys. Rev. B **81**, 212406 (2010).
[60] A. Yoshimori, J. Phys. Soc. Jpn. **14**, 807 (1959).
[61] H. Sato, T. Enoki, M. Isobe, and Y. Ueda, Phys. Rev. B **61**, 3563 (2000).
[62] A. A. Bolzan, C. Fong, B. J. Kennedy, and C. J. Howard, Aust. J. Chem. **46**, 939 (1993).
[63] J. S. Lim, D. Saldana-Greco, and A. M. Rappe, Phys. Rev. B **94**, 165151 (2016).
[64] T. Kimura, J. C. Lashley, and A. P. Ramirez, Phys. Rev. B **73**, 220401(R) (2006).
[65] S. Picozzi, K. Yamauchi, B. Sanyal, I. A. Sergienko, and E. Dagotto, Phys. Rev. Lett. **99**, 227201 (2007).